HIGGS PRODUCTION AT NNLO IN VBF*

J. Cruz-Martinez

Institute for Particle Physics Phenomenology, Durham University
Durham DH1 3LE, UK
j.m.cruz-martinez@durham.ac.uk

(Received June 27, 2018)

This paper expands on recently published results for the factorising next-to-next-to-leading order (NNLO) QCD corrections to Higgs production in the vector boson fusion (VBF) channel. The calculation is fully differential in the kinematics of the Higgs boson and the final-state jets, and is implemented in the NNLOjet framework for computing higher order QCD corrections. We find the NNLO corrections to be limited in magnitude to about $\pm 5\%$ with a weak kinematical dependence in the transverse momenta and rapidity separation of the two tagging jets.

DOI:10.5506/APhysPolBSupp.11.277

1. Introduction

The discovery of the Higgs boson at the CERN Large Hadron Collider (LHC) [1,2] has initiated an intensive program of precision measurements of the Higgs boson properties and of its interactions with all other elementary particles. A large spectrum of Higgs boson decay modes and production channels are being investigated at the LHC. The Higgs boson can be produced at hadron colliders [3] either through its Yukawa coupling to the top quark or through its coupling to the electroweak gauge bosons. This electroweak coupling gives rise to two production modes: associated production with a vector boson, and vector boson fusion (VBF).

At the LHC energies, the VBF process is the second-largest inclusive production mode for Higgs bosons, amounting to about 10% of the dominant gluon fusion process. The detailed experimental study of the VBF production mode probes the electroweak coupling structure of the Higgs boson, thereby testing the Higgs mechanism of electroweak symmetry breaking.

* Presented at the Final HiggsTools Meeting, Durham, UK, September 11–15, 2017.

Perturbative corrections to Higgs boson production in VBF have been derived at next-to-leading order (NLO) in QCD [4–7] and in the electroweak theory [8]. NNLO QCD corrections to the inclusive VBF Higgs production cross section were found to be very small [9], they are further improved by third-order (N3LO) corrections [10].

In contrast, our implementation of this process at NNLO in NNLOjet [11,12] is fully differential in all kinematical variables and, therefore, it allows us to compute any IR-safe observable at this order.

1.1. VBF cuts

The Born-level VBF process consists of two independent quark lines, each emitting an electroweak gauge boson, linked through an HWW or HZZ vertex, as depicted in Fig. 1. The lack of colour exchange between the two initial-state partons means that hadronic activity in the central region is suppressed with respect to other important Higgs production channels, where the complicated colour structure means that radiation in the central region is enhanced. Precisely, this feature lies at the heart of the VBF cuts designed to single out VBF over other production modes [13, 14]. Besides enhancing the relative contribution of VBF processes, the VBF cuts also strongly suppress interference effects between both quark lines, which are present for identical quark flavours.

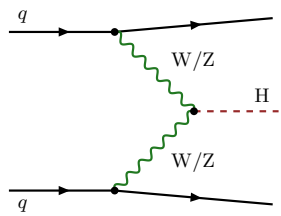

Fig. 1. Born-level vector boson fusion process.

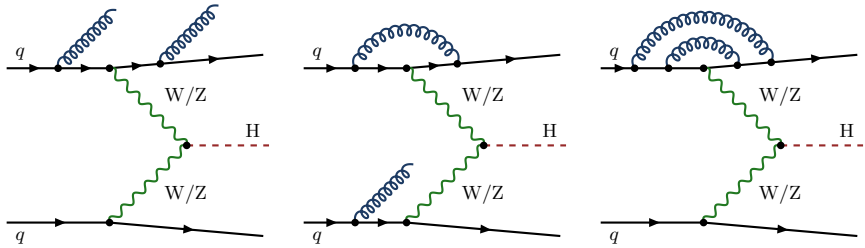

Fig. 2. Examples of second order QCD corrections (RR, RV, VV) to the VBF process.

When computing higher order QCD corrections, one can exploit this Born-level factorisation of the VBF process into two independent quark lines. Due to colour conservation, a single gluon exchange is forbidden between the quark lines, such that NLO corrections can be computed by considering corrections to the each quark line independently. Since each single quark line in the VBF process is identical to the deeply inelastic scattering (DIS) process of a quark on a vector boson current, this factorisation into two independent processes is also called the "structure function approach" [15]. Beyond NLO, one can define the structure function approach by forbidding colour exchange between the quark lines. This results in a gauge-invariant subset of diagrams. Several studies have been performed, showing that the contributions that are neglected in the structure function approach are very small in the relevant phase-space regions defined by VBF cuts, even if they are sizeable when no cuts are used [8, 16, 17]. Interference effects between the VBF production channel and other production channels are also negligible [18].

For our numerical computations, we select events in which the two tagging jets are encountered in different hemispheres, with a rapidity gap between them of $\Delta y_{jj} > 4.5$. A cut on the invariant mass of the two tagging jets of $M_{jj} > 600$ GeV further suppresses s-channel contributions [19]. Jets are defined using the anti-k_t algorithm [20] with a radius parameter $R = 0.4$ and are required to have a transverse momentum greater than 25 GeV and a rapidity of under 4.5. This rapidity condition ensures both tagging jets are found in opposite hemispheres.

We can summarise the VBF cuts as

$$\begin{aligned} p_{\mathrm{T}_j} &> 25\ \mathrm{GeV}\,, & |y_j| &< 4.5\,, \\ M_{jj} &> 600\ \mathrm{GeV}\,, & \Delta y_{jj} = |y_{j_1} - y_{j_2}| &> 4.5\,, \end{aligned} \tag{1}$$

which are the same cuts as used in Refs. [11] and [21].

These cuts are designed to single out VBF over other production modes [13, 14] and exploit the lack of colour exchange between the two initial-state partons. This means activity in the central region is suppressed with respect to other Higgs production channels. Besides enhancing the relative contribution of VBF-like processes, these cuts also suppress interference effects between both quark lines (present for identical quark flavours).

2. NNLOjet

QCD NNLO corrections include contributions from double real radiation (RR), single real radiation at one loop (RV) and two-loop virtual (VV), which introduce implicit infrared (IR) singularities (upon phase-space integration) and explicit IR poles (from loop integrals) which need to be regulated. In order to render each contribution finite and numerically integrable,

we use the antenna subtraction technique [22–25] for the subtraction of real radiation singularities and the reintroduction of its integrated counterparts

$$\begin{aligned} \mathrm{d}\sigma^{\mathrm{NNLO}} &= \int_{\Phi_5} \mathrm{d}\sigma^{\mathrm{RR}} + \int_{\Phi_4} \mathrm{d}\sigma^{\mathrm{RV}} + \int_{\Phi_3} \mathrm{d}\sigma^{\mathrm{VV}} \\ &= \int_{\Phi_5} \left(\mathrm{d}\sigma^{\mathrm{RR}} - \mathrm{d}\sigma^{\mathrm{S}}\right) + \int_{\Phi_4} \left(\mathrm{d}\sigma^{\mathrm{RV}} - \mathrm{d}\sigma^{\mathrm{T}}\right) + \int_{\Phi_3} \left(\mathrm{d}\sigma^{\mathrm{VV}} - \mathrm{d}\sigma^{\mathrm{U}}\right) , \end{aligned} \tag{2}$$

where the integration is over the additional phase space of the radiated partons.

The numerical parton-level implementation is performed in the Fortran-based NNLOjet framework [12], which provides the phase-space generator, event handling and analysis routines as well as subroutines for all unintegrated and integrated antenna functions used to construct (and are common to all processes implemented in NNLOjet).

The process-dependent Fortran code for the various subtraction terms (which need to be manually coded in Maple), different parton orderings and prefactors stemming from symmetries and colour configurations is autogenerated using Maple.

For our numerical computations, we use LHAPDF [26] with the NNPDF3.0 parton distribution functions [27] with the value of $\alpha_{\mathrm{s}}(M_Z) = 0.118$[1], and $M_H = 125$ GeV, which is compatible with the combined results of ATLAS and CMS [28]. Furthermore, we use the following electroweak parameters as input:

$$\begin{aligned} M_W &= 80.398 \text{ GeV}, & \Gamma_W &= 2.141 \text{ GeV}, \\ M_Z &= 91.188 \text{ GeV}, & \Gamma_Z &= 2.495 \text{ GeV}. \end{aligned} \tag{3}$$

The central value for the renormalisation and factorisation scales are chosen as suggested in [21]

$$\mu_0^2 \left(p_{\mathrm{T}}^H\right) = \frac{M_H}{2} \sqrt{\left(\frac{M_H}{2}\right)^2 + \left(p_{\mathrm{T}}^H\right)^2} . \tag{4}$$

3. Results

Table I lists the total fiducial cross section with and without VBF cuts. It is important to note that the VBF cuts increase the size of the NLO and NNLO effects, which can be up to three times larger than what is found in the fully inclusive case.

[1] `NNPDF30_nnlo_as_0118`.

TABLE I

Total VBF-2j cross section with and without VBF cuts. The uncertainty corresponds to a scale variation of $\mu_F = \mu_R = \{\frac{1}{2}, 1, 2\} \times \mu_0$. μ_0 is given in Eq. (4).

	$\sigma^{\text{inclusive}}$ [fb]	$\sigma^{\text{VBF cuts}}$ [fb]
LO	4032^{+56}_{-69}	957^{+66}_{-59}
NLO	3927^{+25}_{-24}	877^{+7}_{-17}
NNLO	3884^{+16}_{-12}	844^{+9}_{-9}

Differential distributions also show some dependence on the cuts. Figure 3 (a) shows the transverse momentum distribution of the Higgs boson (p_T^H). The NNLO corrections for lower values of the observable are moderate (around -5%) and lie outside the NLO scale uncertainty band. For medium and high momenta, the NNLO contribution becomes almost negligible and is contained within the NLO uncertainty band.

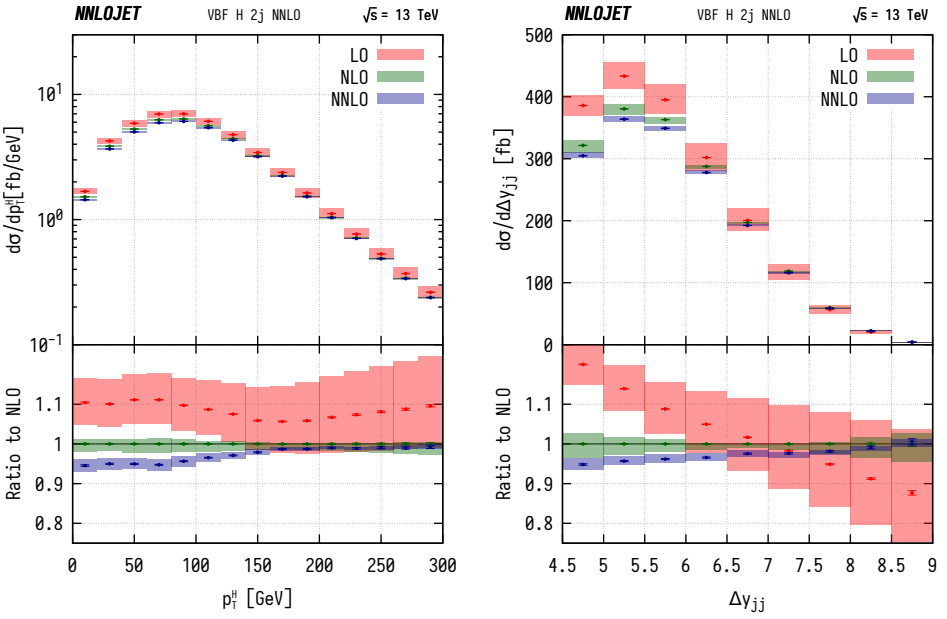

(a) Higgs boson transverse momentum distribution in VBF process

(b) Rapidity gap between the two tagging jets

Fig. 3. Differential distributions applying the VBF cuts of Eq. (1).

Similar features can be observed in Fig. 3 (b) where we present the spatial distribution of the tagging jets as described by their separation in rapidity (Δy_{jj}). For the range of $\Delta y_{jj} \in [4.5, 7]$, which accounts for the bulk of the cross section, the NNLO contribution lies outside the NLO scale bands, whereas for higher values of the observable, the scale uncertainty bands overlap. The NNLO correction, however, remains small over the entire considered range.

The transverse momentum distributions of the leading and subleading jets (the two tagging jets) are shown in Fig. 4. We observe that the NLO and NNLO corrections are both less uniform than the Higgs transverse momentum, they change from positive or negligible for low momenta to negative for medium or large transverse momentum, where the scale bands once again completely overlap.

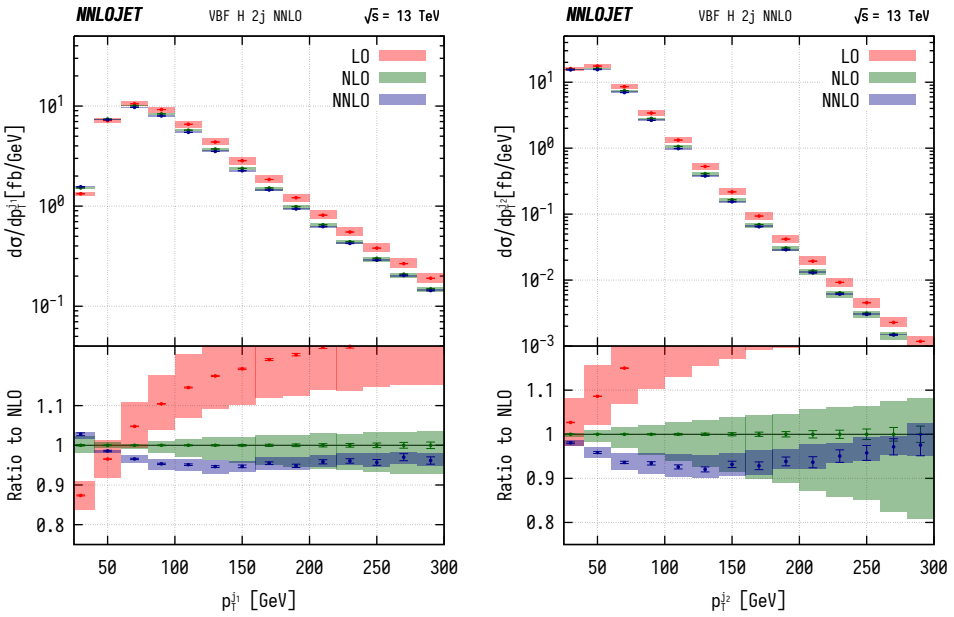

(a) Transverse momentum distribution of the leading jet in VBF

(b) Transverse momentum distribution of the subleading jet in VBF

Fig. 4. Differential distributions applying the VBF cuts of Eq. (1).

The magnitude of the NNLO corrections is, in general, moderate, and very rarely exceeds 5%, while the NLO corrections can be as large as 30% and lead to a substantial modification of the shape of the distributions. Despite partly lying outside the uncertainty bands in the range of the observables we consider, the small magnitude of the NNLO corrections and scale uncertainty bands indicates a good perturbative convergence.

The NNLO QCD corrections for VBF-2j production were first computed in [21], using the Projection-to-Born method applied to the NLO VBF-3j calculation of Ref. [29]. We found [11] a very large discrepancy for the NNLO QCD contribution with respect to [21]. This led to the identification of an error in the NLO VBF-3j calculation of [29]. Once this error was corrected, we found an excellent agreement with the revised results of [21].

4. Conclusions

We computed the second-order QCD corrections to Higgs boson production through Vector Boson Fusion in the DIS approximation which has been proven to be a very reliable approximation when VBF cuts are applied. Our results are implemented and validated in the NNLOJET framework and can be used to compute any infrared-safe observable derived from the VBF process up to $\mathcal{O}\left(\alpha_s^2\right)$.

We observe a kinematical dependence of the NNLO corrections only in the distributions of the two leading jets (tagging jets) in transverse momentum and rapidity separation, usually amounting to no more than a 5% correction. Since it is precisely through cuts on these variables that the VBF process is defined, the NNLO effects may have an important impact on the precise efficiency of the VBF cuts, and consequently on all future precision studies of VBF Higgs boson production.

REFERENCES

[1] G. Aad *et al.* [ATLAS Collaboration], *Phys. Lett. B* **716**, 1 (2012) [arXiv:1207.7214 [hep-ex]].

[2] S. Chatrchyan *et al.* [CMS Collaboration], *Phys. Lett. B* **716**, 30 (2012) [arXiv:1207.7235 [hep-ex]].

[3] A. Djouadi, *Phys. Rep.* **457**, 1 (2008) [arXiv:hep-ph/0503172].

[4] T. Figy, C. Oleari, D. Zeppenfeld, *Phys. Rev. D* **68**, 073005 (2003) [arXiv:hep-ph/0306109].

[5] E.L. Berger, J.M. Campbell, *Phys. Rev. D* **70**, 073011 (2004) [arXiv:hep-ph/0403194].

[6] T. Figy, D. Zeppenfeld, *Phys. Lett. B* **591**, 297 (2004) [arXiv:hep-ph/0403297].

[7] K. Arnold *et al.*, *Comput. Phys. Commun.* **180**, 1661 (2009) [arXiv:0811.4559 [hep-ph]].

[8] M. Ciccolini, A. Denner, S. Dittmaier, *Phys. Rev. D* **77**, 013002 (2008) [arXiv:0710.4749 [hep-ph]].

[9] P. Bolzoni, F. Maltoni, S.-O. Moch, M. Zaro, *Phys. Rev. Lett.* **105**, 011801 (2010) [arXiv:1003.4451 [hep-ph]].

[10] F.A. Dreyer, A. Karlberg, *Phys. Rev. Lett.* **117**, 072001 (2016) [arXiv:1606.00840 [hep-ph]].

[11] J. Cruz-Martinez, T. Gehrmann, E.W.N. Glover, A. Huss, *Phys. Lett. B* **781**, 672 (2018) [arXiv:1802.02445 [hep-ph]].

[12] T. Gehrmann *et al.*, arXiv:1801.06415 [hep-ph].

[13] V.D. Barger, R.J.N. Phillips, D. Zeppenfeld, *Phys. Lett. B* **346**, 106 (1995) [arXiv:hep-ph/9412276].

[14] D.L. Rainwater, D. Zeppenfeld, K. Hagiwara, *Phys. Rev. D* **59**, 014037 (1998) [arXiv:hep-ph/9808468].

[15] T. Han, G. Valencia, S. Willenbrock, *Phys. Rev. Lett.* **69**, 3274 (1992) [arXiv:hep-ph/9206246].

[16] F. Campanario, T.M. Figy, S. Plätzer, M. Sjödahl, *Phys. Rev. Lett.* **111**, 211802 (2013) [arXiv:1308.2932 [hep-ph]].

[17] P. Bolzoni, F. Maltoni, S.-O. Moch, M. Zaro, *Phys. Rev. D* **85**, 035002 (2012) [arXiv:1109.3717 [hep-ph]].

[18] J.R. Andersen, T. Binoth, G. Heinrich, J.M. Smillie, *J. High Energy Phys.* **0802**, 057 (2008) [arXiv:0709.3513 [hep-ph]].

[19] D. de Florian *et al.* [LHC Higgs Cross Section Working Group], arXiv:1610.07922 [hep-ph].

[20] M. Cacciari, G.P. Salam, G. Soyez, *J. High Energy Phys.* **0804**, 063 (2008) [arXiv:0802.1189 [hep-ph]].

[21] M. Cacciari *et al.*, *Phys. Rev. Lett.* **115**, 082002 (2015) [*Erratum ibid.* **120**, 139901 (2018)] [arXiv:1506.02660 [hep-ph]].

[22] A. Gehrmann-De Ridder, T. Gehrmann, E.W.N. Glover, *J. High Energy Phys.* **0509**, 056 (2005) [arXiv:hep-ph/0505111].

[23] A. Gehrmann-De Ridder, T. Gehrmann, E.W.N. Glover, *Phys. Lett. B* **612**, 49 (2005) [arXiv:hep-ph/0502110].

[24] A. Gehrmann-De Ridder, T. Gehrmann, E.W.N. Glover, *Phys. Lett. B* **612**, 36 (2005) [arXiv:hep-ph/0501291].

[25] A. Daleo, T. Gehrmann, D. Maitre, *J. High Energy Phys.* **0704**, 016 (2007) [arXiv:hep-ph/0612257].

[26] A. Buckley *et al.*, *Eur. Phys. J. C* **75**, 132 (2015) [arXiv:1412.7420 [hep-ph]].

[27] R.D. Ball *et al.*, [NNPDF Collaboration], *J. High Energy Phys.* **1504**, 040 (2015) [arXiv:1410.8849 [hep-ph]].

[28] G. Aad *et al.*, [ATLAS, CMS collaborations], *Phys. Rev. Lett.* **114**, 191803 (2015) [arXiv:1503.07589 [hep-ex]].

[29] T. Figy, V. Hankele, D. Zeppenfeld, *J. High Energy Phys.* **0802**, 076 (2008) [arXiv:0710.5621 [hep-ph]].